Nanoscale

Fully atomistic molecular dynamics modeling of photoswitchable azo-PC lipid bilayers: structure, mechanical properties, and drug permeation

Journal:	*Nanoscale*
Manuscript ID	NR-ART-06-2024-002509.R1
Article Type:	Paper
Date Submitted by the Author:	03-Nov-2024
Complete List of Authors:	Alberto, Kevin; University of Texas at Dallas, Chemistry and Biochemistry
Mohammed Nazar, Hasna Begam; The University of Texas at Dallas, Chemistry and Biochemistry
Xiong, Hejian; Southern Medical University, School of Basic Medicine
Shinoda, Wataru; Okayama University, Department of Chemistry
Slesinger, Paul A.; Icahn School of Medicine at Mount Sinai
Qin, Zhenpeng; University of Texas at Dallas, Mechanical Engineering and Bioengineering; University of Texas Southwestern Medical Center at Dallas, Department of Surgery
Nielsen, Steven; University of Texas at Dallas, Chemistry & Biochemistry

SCHOLARONE™
Manuscripts

Journal Name

Fully atomistic molecular dynamics modeling of photo-switchable azo-PC lipid bilayers: structure, mechanical properties, and drug permeation[†]

Kevin A. Alberto,[a] M. N. Hasna Begam,[a] Hejian Xiong,[b] Wataru Shinoda,[c] Paul A. Slesinger,[d] Zhenpeng Qin,[e] and Steven O. Nielsen [*a]

Phospholipid based vesicles called liposomes are commonly used as packaging in advanced drug delivery applications. Stimuli-responsive liposomes have been designed to release their contents under certain conditions, for example through heating or illumination. However, in the case of photosensitive liposomes based on azo-PC, namely phosphatidylcholine lipids with azobenzene incorporated into one of the two lipid tails, the release mechanism is not known. Here we show, using fully-atomistic molecular dynamics simulations of pure azo-PC bilayers, that drug permeation through the bilayer is driven by a light-induced gel-to-liquid lipid phase transition that softens the membrane bending rigidity by an order of magnitude, increases the area per lipid, and decreases the membrane thickness. Furthermore, using phenol as a model drug, we quantified its translocation free energy and its ability to cross the bilayer as a result of a chemical potential gradient induced through a double-bilayer simulation unit cell. The molecular level structural and dynamic information obtained in this study should be of help in designing new azo-PC based liposomes.

1 Introduction

Phospholipid-based vesicles are used by cells to transport material between subcellular organelles. They are also used to transport material out of the cell and to accept and transport material coming into the cell. This biological function of lipid vesicles is the inspiration for liposome-based drug delivery techniques, which aim to transport drugs to where they are needed in the body by packaging them in artificial vesicles called liposomes. Typical injected or injested drug treatments lack specificity, requiring high doses and often produce unwanted side effects. Liposomal drug delivery strategies attempt to overcome this lack of specificity.

Vesicles display specific proteins on their surface that recognize and fuse only with their intended target organelle membrane. For liposomes, this would mean targeting specific cells through the incorporation of recognition proteins or other molecules such as aptamers, folic acid, or carbohydrates. However, of the 14 liposomal products approved by the U.S. Food and Drug Administration and European Medicines Agency as of 2022[1], only two of them use such targeting molecules: AmBisome uses amphotericin B to target fungi and Shingrix uses glycoproteins for antibody B cell response.[2] The others simply take advantage of altered drug pharmacokinetics and pharmacodynamics due to the liposomal formulation.

Motivated by numerous difficulties with a targeting molecule strategy, Yatvin et al. proposed a different approach: liposomes that are designed to release their contents upon heating.[3] Such thermosensitive liposomes are designed to release encapsulated cargo in a specific region heated by radiofrequency or ultrasound. Heating above the lipid melting transition temperature (T_m) changes the membrane from the ordered gel L_o state to the disordered fluid L_α state. This transition leads to an increase in the permeability of the membrane and drug molecules can thus easily cross the membrane.[1] It has also been suggested that near T_m liposomes become leaky due to disorder at the boundary between the solid and fluid domains[4].

Yatvin et al.[3] tuned T_m in the range 41-54 °C by mixing DPPC ($T_m = 41$ °C) and DSPC ($T_m = 54$ °C) in various ratios. Needham et

[a] Department of Chemistry and Biochemistry, The University of Texas at Dallas, Richardson, TX 75080, USA; E-mail: steven.nielsen@utdallas.edu
[b] Guangdong-Hong Kong-Macao Greater Bay Area Center for Brain Science and Brain-Inspired Intelligence, Department of Neurobiology, School of Basic Medical Sciences, Southern Medical University, Guangzhou, China.
[c] Research Institute for Interdisciplinary Science, Okayama University, Okayama 700-8530, Japan.
[d] Nash Family Department of Neuroscience, Icahn School of Medicine at Mount Sinai, New York, NY 10029 USA.
[e] Department of Mechanical Engineering, The University of Texas at Dallas, Richardson, TX 75080, USA.
[†] Supplementary Information available: All the files needed to run NAMD molecular dynamics simulations of the trans-azo-PC and cis-azo-PC lipid bilayer systems are included. See DOI: 00.0000/00000000.

al.[5] added lysolipid to the thermosensitive liposome composition which enhances cargo release putatively by forming pores at the solid/liquid domain boundaries.[6]

Another paradigm for triggering drug release is to use light, namely to design photosensitive liposomes. Typically in such systems the application of light results in irreversible changes to the liposome.[7] The exception is lipid molecules containing azobenzene that undergo reversible *cis-trans* isomerization. UV light causes isomerization in the *trans* to *cis* direction, while blue light causes isomerization in the opposite direction. The *cis* to *trans* isomerization also occurs spontaneously but over a longer time scale. In their review of the use of liposomes in biosensing, Mazur et al.[8] point out that lysis of the liposomes is usually required to output an enzymed-based, fluorescence-based, or other signal; the use of photo-sensitive liposomes in these applications could open up more possibilities. Also, in the "new paradigms for the future" section of their review article on the role of liposomes in nanomedicine, Crommelin et al.[9] discuss the importance of triggering drug release from liposomes, of which light activation is one possibility. In a more ambitious study, Zhao et al.[10] designed an artificial lipid-based molecular machine composed in part of photoisomerable azobenzene-based lipidoids which convert light energy into mechanical movements to disrupt endo-lysosomal compartments and hence deliver cargo to the cytosol of cells.

Morgan et al.[11] introduced azo-PC, a synthetic phosphatidyl-choline derivative which contains a photoisomerizable azobenzene moiety in one of the two lipid tails, and mixed it with DPPC to make such reversible photosensitive liposomes. More recently, Chander et al. incorporated azo-PC into lipid vesicles to deliver doxorubicin,[12] while Xiong et al. used lipid vesicles containing azo-PC to deliver a dopamine D1-like receptor agonist to striatal neurons and coined this class of lipid nanocarriers "azosomes"[13]. This term will be used throughout the remainder of this paper in reference to azo-PC containing liposomes. The ability of azosomes to deliver different molecules for various purposes shows the potential wide application of these nanocarriers. Additionally, azosomes exhibit high spatiotemporal control since an external light stimulus is used to release their contents.

The release mechanism of cargo from azosomes is unclear. Morgan et al.[11] reported that azosomes made of DPPC and azo-PC are more permeable to water after UV irradiation; however their calcein-loaded azosomes showed no dye leakage. Xiong et al.[13] reported calcein release upon UV irradiation in azosomes constituting azo-PC, DSPE-PEG2000, DSPC, and cholesterol; the release was switched off upon irradiation with blue light. Pritzl et al.[14] reported ATTO-532 dye leakage after photoswitching both with UV and with blue light in pure azo-PC azosomes; they attribute permeability to transient pore formation supported by patch clamp data using chloride ions, but it is not clear if small chloride ions would permeate with a similar mechanism to fluorescent dyes.

These contrasting results, namely no leakage, leakage only in the *trans* to *cis* switching direction, and leakage in both directions, come from azosomes of different lipid compositions. Domain formation could possibly be implicated in these differing

observations. Morgan et al.[11] postulated that the equilibrium distribution of *cis* and *trans* azo-PC isomers within the bilayer might be different in mixed azo-PC/DPPC bilayers below the thermal phase transition temperature on the basis of their data. Urban et al.[15] reported membrane domains in azosomes composed of *trans*-azo-PC, diphytanoylphosphocholine (DPhPC), and cholesterol which disappear upon *trans*-to-*cis* isomerization and reform again after *cis*-to-*trans* isomerization. Even in the case of pure azo-PC azosomes, since Pritzl et al.[14] apply blue light shortly after applying UV light to observe dye release in both instances, when the blue light is applied the azosomes are presumably in a mixture of *trans*-azo-PC and *cis*-azo-PC, which in principle could phase separate from one another.

To better understand the mechanisms of release with azosomes, in this study we focus on molecular dynamics simulations of pure azo-PC bilayers. Our results suggest that *trans*-azo-PC is in a gel-like phase, while *cis*-azo-PC is in a liquid-disordered phase, irrespective of the temperature. Thus, *trans*-to-*cis* isomerization results in a gel-to-liquid phase transition that increases the bilayer permeability without the application of heat. This is consistent with the study by Mathai et al. showing that the strongest indicator of water permeability across lipid bilayers is the area per lipid[16].

We found that the *trans*-to-*cis* isomerization caused a reversible increase in the area per lipid, a decrease in bilayer thickness, a decrease in the bending modulus, and a drastically different hydrophobic core structure, all of which help to reduce the energy barrier for a molecule permeating across the *cis* membrane. We tested permeation with phenol as a model drug, and with SKF-81297 (6-chloro-2,3,4,5-tetrahydro-1-phenyl-1H-3-benzazepine-7,8-diol) as a real drug, using both single and double bilayer unit cells. Our detailed results follow.

2 Simulation and Analysis Methods

The initial bilayers of 64 lipids per leaflet were created using packmol[17]. The azobenzene isomer state was controlled by the C-N-N-C torsion potential and the respective atoms are highlighted in Figure 1. The azobenzene parameters by Böckmann et al.[18] were modified by Siriwardane et al.[19] to maintain a single isomeric state by creating energy minima corresponding to a particular isomer and an extremely high energy barrier which prevents conversion between isomers. These potential energy functions are shown in Figure 4.

Additionally, the "extra bonds" functionality in NAMD can be used to choose the isomer state for each lipid molecule. To create the azo-PC topology, a new entry was created by modifying the existing DSPC topology[20] to incorporate the azobenzene moiety. Existing CHARMM36 lipid parameters[20] were used when possible, and any missing parameters were obtained from the CGenFF server[21-24]. All simulations were performed with NAMD under the tensionless ensemble at 323 K and 1 atm with periodic boundaries enabled in each direction.[25] The NAMD implementation of the TIP3P water model was used to solvate the systems.[26] The SKF-81297 parameters were obtained from the CGenFF web server and used without modification. Of note, the SKF-81297 model used the halogen bond improvement to the CHARMM
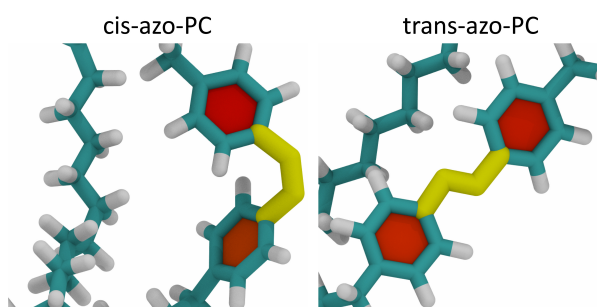
cis-azo-PC   trans-azo-PC

Fig. 1 Highlight of the azobenzene torsion in *cis*-azo-PC and *trans*-azo-PC. The corresponding C-N-N-C atoms are highlighted in yellow.

general force field by Gutiérrez *et al.*[27] Visualization and image rendering was done in VMD, and post-simulation analysis was performed with custom Python scripts utilizing the MDAnalysis Python package[28–30].

2.1 Area Per Lipid

APL is a useful quantity to help monitor the bilayer structural changes upon isomerization. The area per lipid (APL) was calculated using Equation 1 from the periodic cell dimensions collected every 1 ps. The full data was used to generate Figure 4, however, the first 20 ns after an isomer switch was ignored when calculating the APL. In this work, the APL has been calculated as

$$APL = \frac{L_X L_Y}{N_L} \qquad (1)$$

where L_X and L_Y are the simulation cell dimensions in the X- and Y-directions, respectively, and N_L is the number of lipids per leaflet. Unless otherwise noted, the simulated bilayers had 64 lipids per leaflet. At this unit cell size membrane undulations are not significant so that Equation 1 is sufficient to calculate the APL.

2.2 Free Energy Profile Calculations

Adaptive biasing force (ABF) MD simulations were used to obtain the free energy profile of a phenol molecule, and an SKF molecule, across a pure azo-PC bilayer for each isomer. The z-distance from the bilayer center (midplane) was used as the reaction coordinate using the collective variables module in NAMD.[31] Six different windows were used for the ABF simulations: $|z| = 0 - 6$ Å, $6 - 12$ Å, $12 - 18$ Å, $18 - 24$ Å, $24 - 30$ Å, and $30 - 36$ Å. Each window was run for 400 ns for phenol and 600 ns for SKF. Sampling was performed over half of the membrane, and the resulting free energy profile was symmetrized.

2.3 Double Bilayer

Double bilayer systems of azo-PC and phenol or SKF-81297 as the permeant were simulated under the tensionless ensemble at 323 K and 1 atm. To create the double bilayer systems, an equilibrated single bilayer of 64 azo-PC lipids per leaflet was replicated in the Z-direction and recentered about the origin using the *replicatemol* function in the TopoTools plugin for VMD[30,32]. Due to the increased APL of *cis*-azo-PC, and resultant bilayer thinning,

additional water was added to the *cis* system to prior to replication to prevent interaction between bilayers as well as with their Z-direction periodic images. 100 total phenol molecules, and 50 total SKF-81297 molecules, were added to the outer water regions after replication. The photoisomers were kept in the same isomeric state (*trans* or *cis*) throughout the duration of the simulation. The total number of water molecules in each double bilayer system is as follows: *cis* phenol double bilayer: 30160 water molecules; *trans* phenol double bilayer: 15392 water molecules; *cis* SKF double bilayer: 30160 water molecules; *trans* SKF double bilayer: 27775 water molecules.

2.4 Area Expansion Modulus

The area expansion modulus was calculated by plotting the surface tension vs areal change of fixed-area membrane simulations under the NPAT ensemble, analogous to micropipette aspiration experiments.[33] A membrane patch of 64 lipids per leaflet was simulated at different fixed-areas at 323 K and 1 atm for at least 20 ns where only the bilayer normal dimension was allowed to fluctuate. The surface tension was calculated from the pressure tensor collected every 100 fs using the equation:

$$\gamma = L_Z \left(P_{ZZ} - \frac{P_{XX} + P_{YY}}{2} \right) \qquad (2)$$

where γ is the surface tension, P_{XX}, P_{YY}, and P_{ZZ} are the pressures in the X-,Y-, and Z-directions, respectively. The surface tension was plotted as a function of membrane areal change ($\alpha = \Delta A / A_0$). A best-fit line was computed, and its slope was taken as the area expansion modulus.

2.5 Density Profiles

The electron density profile was computed using the VMD Density Profile Tool by Giorgino[34], and the average was computed over the simulation trajectory. The difference between the average peak maxima was taken as the bilayer thickness. The atom density profile was computed by binning the atomic centers-of-mass for a given selection group (total, azobenzene, or headgroup) along the bilayer Z-Distance for a trajectory of a particular isomer.

2.6 Bilayer Void Volume

In this work, the void volume is defined as the unoccupied volume inside the azo-PC bilayer. To calculate the void volume, the simulation cell was divided into 75 slices of equal width along the bilayer normal to ease analysis, and hard sphere test particles with radius of 1.5 Å were randomly inserted in a given slice until 100000 test particles per slice were attempted. The insertion process was repeated for each slice and each frame of the simulation. Simulation atoms were treated as hard spheres with a van der Waals radius of 1.0 Å, regardless of identity. A test particle was accepted to fit if it did not overlap with any simulation atoms. The void volume is proportional to the ratio of accepted test particles to total attempted insertions, as shown in Equation

3:

$$\text{Void Volume}(\text{\AA}^3) = \frac{N_{accept}}{N_{total}} * S \tag{3}$$

where N_{accept} and N_{total} are the number of test particles accepted and the total number of test particles, respectively, and S is the volume of the given bilayer slice. This process was repeated for each frame of the 500-frame simulation trajectory.

2.7 Tilt and Splay Angle

The vector that joins the geometric center of mass of the three terminal carbons on the two lipid chains of the azo-PC molecule to the midpoint between the phosphate and backbone C2 atoms is defined as the local lipid director vector $\vec{t}$. The tilt angle θ is the angle formed by the vector $\vec{t}$ and the positive bilayer normal direction. In order for $\theta = 0$ to reflect a local alignment in which $\vec{t}$ is parallel to the bilayer normal z axis, the tilt angle is defined within the range $[0°; 180°]$. The angular range $[0°; 90°]$ was selected and its probability distribution $P(\theta)$ was plotted. The angular interval was selected to represent the best-sampled angular region. In this case for the trans bilayer the θ in the range $[10°; 40°]$ and cis bilayer $[0°; 50°]$ are chosen as the best angular intervals.

The angle between the $\vec{t}$ vectors of adjacent lipid molecules is defined as the splay angle, or α. The study was conducted with the same director vector criteria, limiting the analysis to close neighbors by selecting only lipid pairings that were within 10 Å of one another and the best angular intervals chosen from the tilt angle probabilities. The α intervals $[5°; 20°]$ and $[10°; 50°]$ were chosen for the trans and cis bilayers, respectively, since they represent the best-sampled angular regions. Following that, a probability distribution $P(\alpha)$ for the lipids was plotted in the angular range $[0°; 90°]$. The PMF of the form $-k_B T \ln[P(\alpha)/\sin\alpha]$ was computed, fit to a quadratic, and the splay modulus, k_s, is equal to double the quadratic coefficient as shown by Khelashvili et al. [35] The same reference shows the bending rigidity, K_c, is simplified to $K_c = \mathscr{X}_{12}^{LL}$ for a single component membrane, where $\mathscr{X}_{12}^{LL}$ is the splay modulus for the lipid tail-lipid tail pairs.

3 Results and Discussion

Equilibrium simulations at 323 K of pure azo-PC bilayers show that the trans isomer bilayer is in a gel-like state, while the cis isomer bilayer is in a disordered liquid-like state (see Figures 2 and 3). Aside from the obvious structural difference, this terminology was quantified by computing the lipid two dimensional mean squared displacement over time to calculate the self-diffusion constant D_{xy} from $\lim_{t\to\infty}\langle|r_{xy}(t) - r_{xy}(0)|^2\rangle = 4D_{xy}t$. From this analysis we obtained $D_{xy} = 4.6 \times 10^{-8}$ cm^2/s for the cis bilayer and $D_{xy} = 5.3 \times 10^{-9}$ cm^2/s for the trans bilayer which shows that the trans bilayer lipid diffusion constant is roughly one order of magnitude smaller than that of cis. We did not observe a phase transition by changing the temperature; the trans bilayer remains in a gel-like state even above 373 K and the cis bilayer remains in a liquid-like state even below 273 K. However, we could reproducibly change the lipid phase through both trans-to-cis and cis-to-trans isomerization. Specifically, we performed a long simulation in which the isomer state of each lipid was changed every

100 ns (see Figure 4). To accomplish this we used the force field parameters developed by Siriwardane et al. [19] to control the isomer state, in which the C-N-N-C double-well torsional potential is changed into two single-well potentials, one for each isomer (see Figure 4). This reversible switching behavior has been observed experimentally [13,36] and shows that the azosome does not rupture upon isomerization.
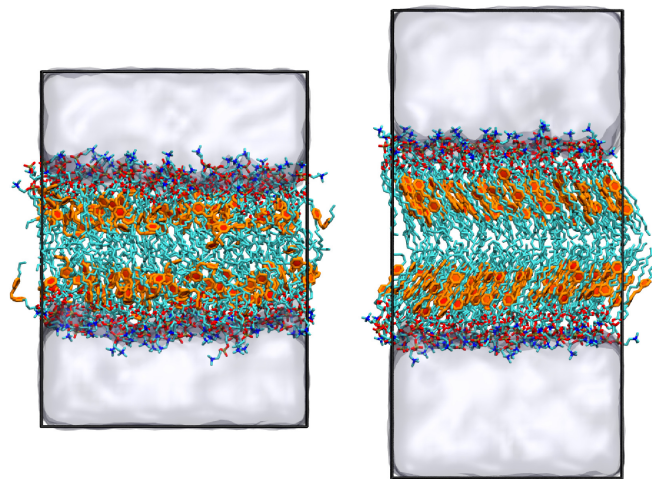

Fig. 2 Snapshots of the pure azo-PC bilayer in 100% cis (left) and trans (right), respectively. The headgroup nitrogen atoms are in blue, the phosphate oxygen and phosphorous atoms are in red and gold, respectively, and the lipid tail carbons are in cyan. The azobenzene groups are represented in orange with their ring planes filled in. Hydrogen atoms have been hidden for clarity. The clear regions represent water, and the simulation cell is drawn in black lines.

In the MD simulations, once the torsional potential is switched the azobenzene isomer state switches on a sub-picosecond time scale and the bilayer structural response is observed (see Figure 4) to occur on the time scale of a few nanoseconds. In the trans-to-cis direction this few nanosecond time scale is expected since the system disorders. However, we were surprised to observe that the ordering (cis-to-trans) transition also occurs quickly and completely.

A striking observation from the MD simulation data is the contrast in the two bilayer structures. The trans-azo-PC bilayer is well-ordered and tightly packed. In contrast, the cis-azo-PC bilayer is disordered and occupies a greater cross sectional area than its trans counterpart. Specifically, the area per lipid increases from 53 Å^2 to 73 Å^2 for the trans-azo-PC and cis-azo-PC bilayers, respectively. We can compare this 37.7% increase in the membrane area from our MD data with recent experimental data. However, it must be pointed out that experimentally not all of the azo-PC lipids are converted to the cis isomer, whereas we have 100% conversion since we set the torsional force field to explic-
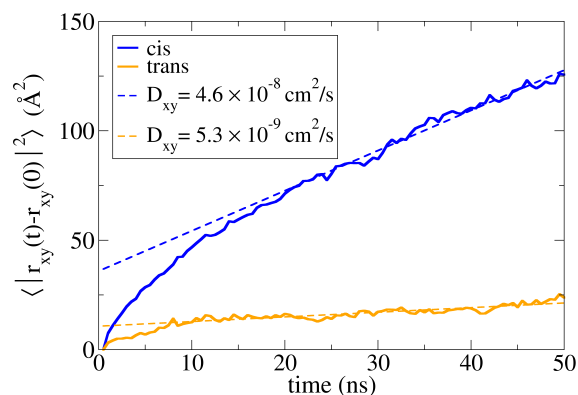
Fig. 3 The lipid lateral mean squared displacement (in the bilayer plane) is calculated separately for the *cis*- and *trans*-azo-PC bilayers from the appropriate segments of the 1400 ns simulation of Fig. 4. This data yields diffusion constants of $D_{xy} = 4.6 \times 10^{-8}$ cm^2/s for the *cis* bilayer and $D_{xy} = 5.3 \times 10^{-9}$ cm^2/s for the *trans* bilayer at 323 K using $\lim_{t \to \infty} \langle |r_{xy}(t) - r_{xy}(0)|^2 \rangle = 4D_{xy}t$ and the shown fitting lines. Note that the fitting lines include the factor of 4 since the slope is $4D_{xy}$.
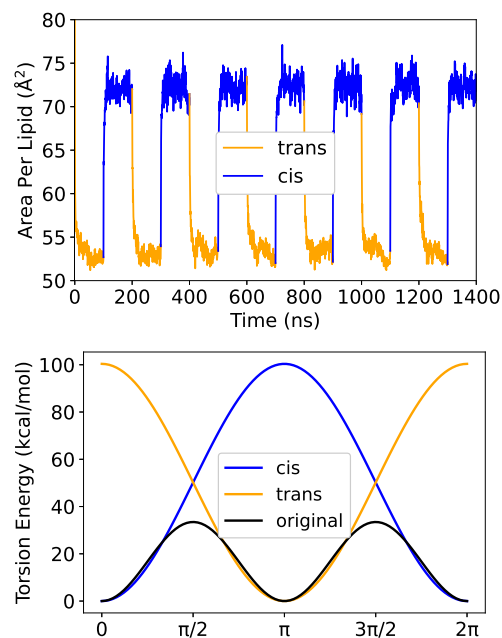

Fig. 4 Left panel: Area per lipid of the azo–PC bilayer over time as the isomer state of each lipid is switched every 100 ns by changing the C-N-N-C torsional force field parameters. Right panel: C-N-N-C torsional potential energy of the original parameters by Böckmann et al. [18] (black) and modified by Siriwardane [19] (blue and orange).

itly destabilize the *trans* state. Specifically, Manafirad et al. [37] show that only 75% of the lipids switch to the *cis* isomer even at high laser intensity, and Ober et al. [38] report a maximum of 83% conversion to the *cis* isomer. In Xiong et al. [13] there are 5 experimental data points for the membrane area increase for 5 different membranes with azo-PC fractions between 0-40%. By extrapolating this data, which is linear, to 100% azo-PC we obtain an area increase value of 28.8%. Then we correct this value assuming that only 75% of the lipids actually switch to the *cis* state, to give a true 100% cis area increase value of 28.8 / 0.75 = 38.4% which compares favorably with our 37.7% MD value. Manafirad et al. [37] report a 19% increase in membrane area for pure azo-PC membranes which can be corrected to a 19 / 0.75 = 25% increase because of incomplete conversion. Aleksanyan et al. [39] report a 20% membrane area increase upon isomerization for pure azo-PC membranes, although they point out that "vesicles made of 100 mol% azo-PC often did not reach perfect elliptical shapes affecting our accuracy for assessing the membrane area increase". Indeed, their 100% value is not on the trend line of their mixed azo-PC / POPC membrane data; by omitting the 100% value, extrapolation of the remaining data to 100% puts the area increase at more than 30% before any correction for incomplete conversion. These data show that the *trans*-to-*cis* isomerization causes a reduction in lipid packing and therefore the *cis*-azo-PC bilayer thins compared to the *trans*-azo-PC bilayer.

The *cis*-azo-PC bilayer has more evenly distributed azobenzene moieties normal to the bilayer plane (relative to the bilayer width, Figure 5), with some even located at the bilayer mid-plane. In contrast, the *trans*-azo-PC bilayer lacks azobenzene moieties near the bilayer mid-plane because of the methyl trough and the strong alignment of the lipid tails. The disordered nature of the *cis*-azo-PC bilayer is further supported by the absence of a methyl trough.

The differing lipid arrangements present in the *trans* and the *cis* azo-PC bilayers are also observed in the electron density profiles (Figure 6). The bilayer thickness, as determined by the peak-to-peak distance of the electron density plot is $d_{HH}^{trans} = 39$Å and $d_{HH}^{cis} = 31$Å consistent with previously reported membrane thickness values. Ober et al. report the dependence of azo-PC bilayer thickness on percent *cis*-azo-PC content. However since they acheive a maximum of 83% conversion to the *cis* isomer, the 100% *cis* value is obtained using the linear regression equation provided in their supporting information; this gives bilayer thickness values of $d_{HH}^{trans} = 40.9$Å and $d_{HH}^{cis} = 30.4$Å. [38] In the recent study by Aleksanyan et al. the reported MD simulation values are $d_{HH}^{trans} = 41$Å, and $d_{HH}^{cis} = 31.2$Å; however the azo-PC lipid they simulated is two carbon atoms shorter in the tail not containing the azobenzene moiety. [39]

To further probe the structural difference between the *cis* and *trans* bilayers, the transient or permanent location of void volume is characterized. Since *trans*-to-*cis* isomerization causes an increase in the area per lipid and a decrease in the bilayer thickness, the bilayer total volume is roughly conserved; however the distribution of void regions may be different.
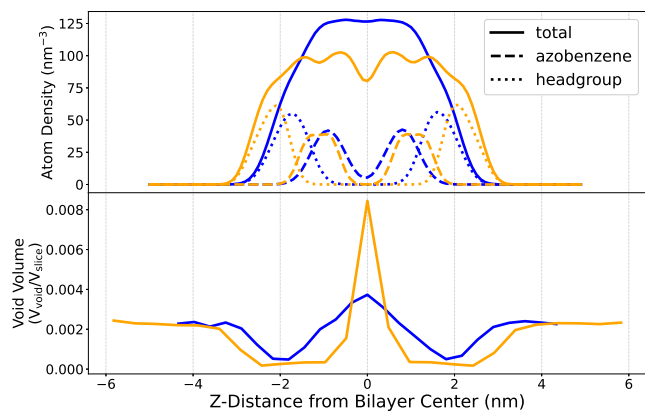
Fig. 5 The atom density (top panel) and free volume (bottom panel) in the azo-PC bilayer as a function of distance along the bilayer normal. The blue and orange lines represent the *cis* and *trans* isomers, respectively.
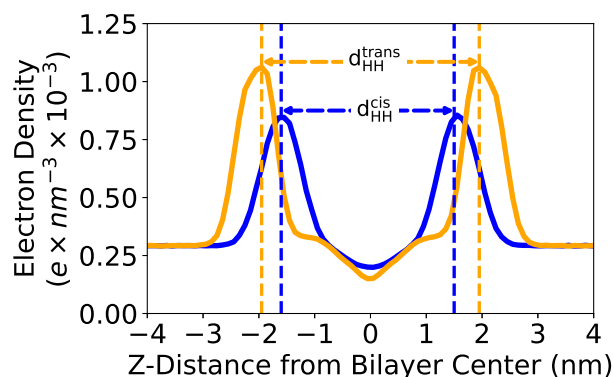

Fig. 6 Pure azo-PC electron density profiles for *cis* (blue) and *trans* (orange), respectively.

As seen in Figure 5, most of the free volume of the *trans* bilayer is localized in the methyl trough region at the bilayer midplane. The *trans* isomer bilayer is thicker, more organized, and has extended regions devoid of free space due to tightly packed lipid tails. In contrast, the free volume is more evenly distributed in the *cis* bilayer, so that one could envisage percolation pathways for small permeants. These data suggest that permeants will have difficulty crossing the *trans* bilayer.

When considering the energetics of possible shape changes in lipid membranes, including membrane deformations and release of drugs, the elastic moduli are critical parameters. High values of the elastic moduli may hinder the controlled release of drugs. We measured an area expansion modulus of $K_A = 210$ mN/m for *trans*-azo-PC and $K_A = 205$ mN/m for *cis*-azo-PC from a plot of membrane surface tension versus cross-sectional area (Figure 7). Aleksanyan et al. report a single area expansion modulus value of $K_A = (221.8 \pm 6.8)$ mN/m using a combined fit as their data did not show any systematic dependence on the azo-PC lipid fraction, or its isomer state, within the bilayer.[39] These K_A data are summarized in Table 1 and fall within the typical range seen for conventional lipids;[40] moreover they are consistent with Mathai's ob-
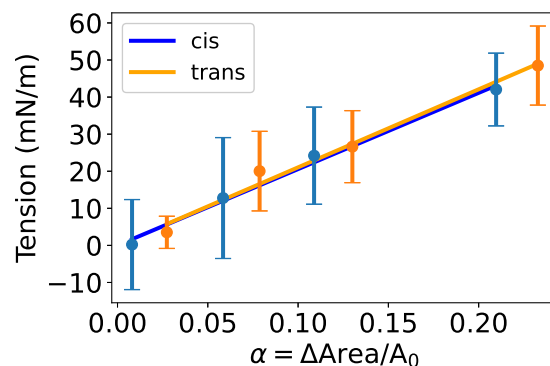

Fig. 7 Fixed area simulations of *cis* (blue) and *trans* (orange) lipid bilayers. The α value on the x-axis is the fractional difference of each fixed area simulation compared to its equilibrium area. Block average standard deviations are used to estimate the error bars.

servations that membrane permeability and area expansion modulus are uncorrelated.[16] Manafirad et al.[37] measured the area expansion modulus of giant unilamellar vesicles composed of mixtures of azo-PC and DOPC using micropipette tensiometry. For the 100% pure azo-PC membranes, they report a value 2.5 times higher for the *trans* bilayer compared to *cis*. But for most of their data set, including the membranes with 80% azo-PC, the area expansion modulus is very similar between the *cis* and *trans* azo-PC isomers. While K_A is important in a membrane's ability to adjust to stress, such as the insertion of a transmembrane protein, it seems to have little importance in predicting membrane permeability.

Table 1 Area per lipid and area expansion modulus. The area per lipid for Aleksanyan et al. is taken from the pdb files they provided

Isomer	Area Per Lipid (Å^2)	K_A (mN/m)
cis-azo-PC (this study)	73	205
trans-azo-PC (this study)	53	210
cis-azo-PC[39]	75.9	222
trans-azo-PC[39]	56.8	222
DPPC[41]	64	231
DSPC[42]	46.8	570

In contrast to the similar area expansion moduli of the *cis*-azo-PC and *trans*-azo-PC bilayers, the *cis*-azo-PC bilayer has an order of magnitude lower bending rigidity than its *trans* counterpart. We computed the bending rigidities from a parabolic fit to the logarithm of the splay angle distribution following the procedure developed by Harries.[35] Whereas the *trans*-azo-PC has a higher bending rigidity of 48.7 kT, indicating a more rigid structure with a smaller potential for shape changes, the *cis*-azo-PC has a lower bending rigidity of 5.3 kT, suggesting better flexibility and ease of deformation in the lipid membrane. In Table 2 we compare our MD data to that of Aleksanyan et al.[39] collected using fluctuation spectroscopy.

3.1 Single Bilayer with Phenol Simulations
Phenol is moderately soluble in water (1.4 mol/L at 323 K[43]), small in size, and its aromatic ring is a common structure of many
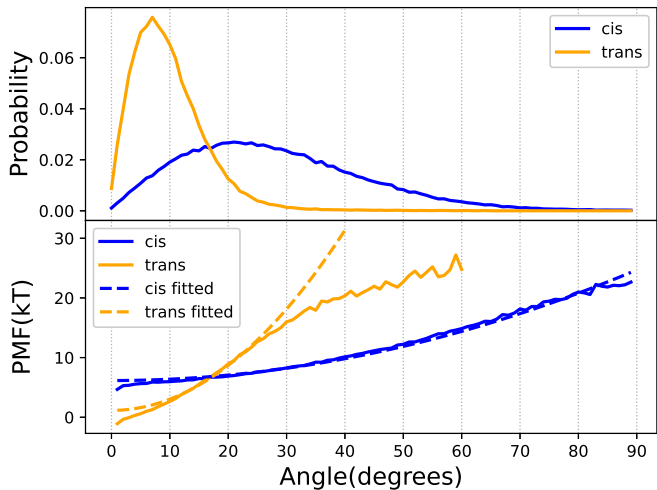
Fig. 8 Top panel: Normalized splay angle probability distributions of *cis*-azo-Pc (blue) and *trans*-azo-PC (orange). Bottom panel: Potential of mean force (PMF) plots for pure azo-PC membranes (*cis* blue and *trans* orange) derived from the splay distributions in top panel and their corresponding quadratic fits.

Table 2 Bending rigidity of pure azo-PC membranes

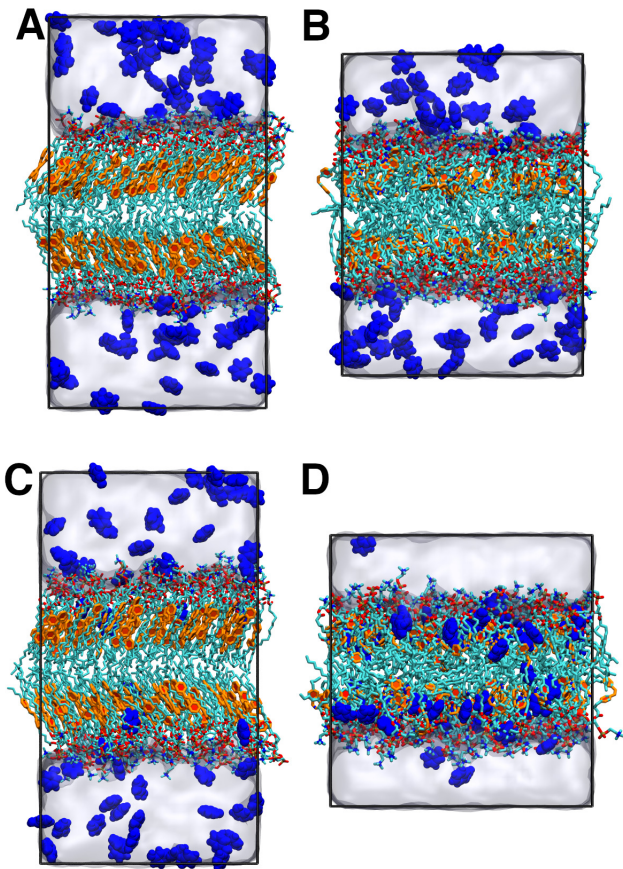| Isomer	Bending rigidity (kT)
cis-azo-PC (this study)	5.3
trans-azo-PC (this study)	48.7
cis-azo-PC[39]	5.4
trans-azo-PC[39]	70.2

Fig. 9 Simulations of phenol interacting with a pure *trans*-azo-PC and pure *cis*-azo-PC bilayer after 1 ns (A and B, respectively) and 25 ns (C and D, respectively). The atoms of the phenol molecules are blue spheres, the *azo*-PC headgroup nitrogen, phoshorous, and carbon atoms are blue, gold, and cyan, respectively. The azobenzene moieties are orange with the ring plane filled in. Hydrogens have been hidden for clarity.

drug and dye molecules; we use it here as a model drug to study its membrane permeability. Specifically, 60 phenol molecules are added to the water phase of the *trans* simulation unit cell and the system was simulated under tensionless bilayer conditions. After 25 ns of simulation, many of the phenol molecules remained in the water phase (Figure 9). However, a very different behavior was observed in the case of the *cis* bilayer; after 25 ns most of the phenol molecules entered the bilayer (Figure 9 D), suggesting that the *cis* bilayer has a much greater ability to accomodate permeants compared to the *trans* bilayer. This behavior is supported by the void volume profile in Figure 5, where the *cis* bilayer can accomodate molecules throughout whereas in the *trans* isomer the void volume is concentrated at the bilayer center so that molecules have to traverse essentially the entire leaflet to get to this region of free volume.

Additionally, when a single phenol molecule is forced to cross the lipid bilayer at a constant velocity using steered molecular dynamics it is seen that in the *trans* bilayer the phenol ring plane tends to orient parallel to the lipid tails whereas in the *cis* bilayer the phenol ring plane has much greater rotational freedom. Snapshots from these translocation simulations are shown in Figure 10.
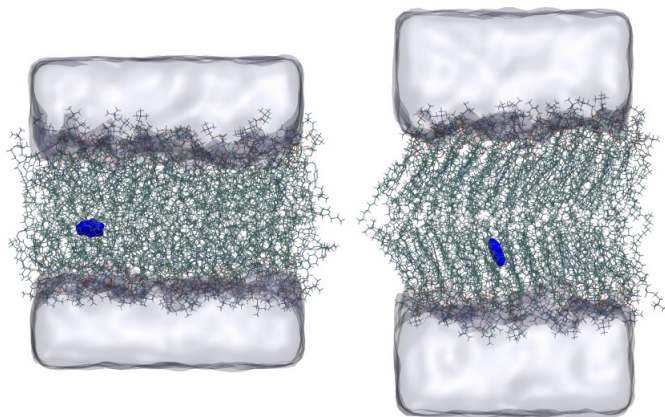
Fig. 10 Snapshots of the orientation of a single phenol molecule (blue spheres) from the constant-velocity SMD simulation of phenol translocation across an azo-PC bilayer in the *cis* (left) and *trans* (right) isomers. The lipid atoms are drawn in cyan lines, and the clear regions represent water.

3.2 Free Energy Profile

To further understand the interaction of phenol with the *cis* and *trans* bilayers, and to study a real drug, namely SKF-81297 which is a dopamine D1-receptor agonist used by Xiong et al. [13], their free energy profiles across the azo-PC bilayers were computed using adaptive biasing force free energy simulations (see Figure 11). No barrier exists for phenol to enter the *cis* membrane. In contrast, for the *trans* membrane a very shallow energy well of 0.3 kcal/mol attracts phenol to the bilayer/water interface, followed by a small barrier of height 0.6 kcal/mol near the location of maximum lipid head group density (see Fig. 5). Inside the membrane, both the phenol free energy minimum and the barrier around the bilayer midplane for the *cis* membrane align with the azobenzene density profile; namely the azobenzene density minimum at the *cis* bilayer midplane in Fig. 5 is correlated with the phenol free energy barrier, and the azobenzene density maximum coincides with the broader phenol free energy minimum. The energy minimum for phenol in the *trans* membrane is 1.85 kcal/mol lower than in bulk water, and this minimum is located between the regions of maximum lipid head group and azobenzene group densities. For phenol in the *cis* membrane the barrier to cross the midplane is 1.8 kcal/mol and the highest overall barrier is 2.6 kcal/mol. Correspondingly, in the *trans* bilayer there is a barrier of 3.1 kcal/mol for phenol to cross the midplane with a shallow well of 0.9 kcal/mol at the midplane where the methyl trough is located. The two additional local minima present in the phenol *trans* bilayer free energy profile, the higher barrier to cross the membrane, and the intrinsically slower dynamics of the *trans* bilayer lipids all contribute to suppress phenol translocation events.

The larger SKF-81297 molecule has a deep energy minimum of around 9 kcal/mol in both azo-PC bilayers indicating that it is lipophilic, which is consistent with its logP value in the 2-3 range. Similar to phenol, there is essentially no barrier for SKF to enter the *cis* membrane, whereas there is a small barrier of 1.1 kcal/mol for SKF to get past the lipid head groups. Near the

bilayer midplane the SKF behavior is also similar to that of phenol; SKF has an additional barrier of 1.8 kcal/mol and a shallow well of 0.5 kcal/mol to cross the midplane. Also, the energy minimum location of SKF in the *trans* membrane coincides with the azobenzene group density maximum.

Despite a propensity for phenol and SKF molecules to enter the *cis* bilayer, there is no reason for them to cross from one side of the bilayer to the other because the two "sides" of the bilayer are actually the same region of space under periodic boundary conditions and furthermore the system is symmetric about the bilayer midplane. Therefore, the single bilayer system is extended to a unit cell including a double bilayer to create a chemical potential gradient that can provide a driving force for molecules to cross from one side of the bilayer to the other as discussed next.
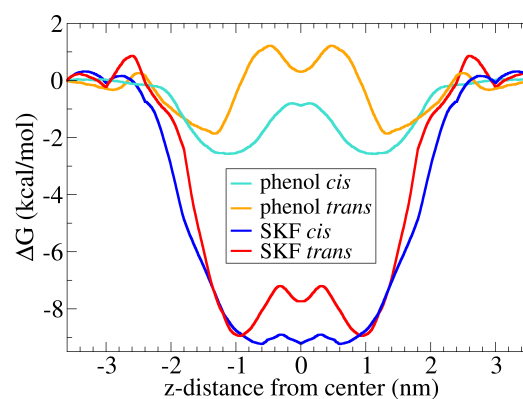

Fig. 11 Free energy profile of phenol and SKF-81297 crossing pure azo-PC *cis* and *trans* bilayers calculated with the adaptive biasing force method.

3.3 Double Bilayer Simulations

In the double bilayer systems with phenol, a total of 100 phenol molecules are initially placed in the outer water region. The snapshots from the simulation trajectories in Figure 12 show clear differences between the phenol permeability of *cis-azo*-PC and *trans-azo*-PC. Phenol is able to permeate across the *cis* bilayer after approximately 25 ns of simulation. Even after 100 ns, phenol failed to permeate across the *trans* bilayer, corroborating the computed free energy profile analysis and consistent with previous observations. [12,13] Thus, two distinct permeability behaviors are observed for the *cis* and *trans* bilayers, which agrees with the experimental results where it was shown that the *trans*-to-*cis* isomerization caused azosomes to release their contents [12,13].

50 SKF molecules were initially placed in the outer water region of both *cis-azo*-PC and *trans-azo*-PC double bilayers. The drug partitions into both the *cis*- and *trans*-azo-PC bilayer membranes since it is lipophilic but on the maximum timescale that we could simulate (500 ns) we do not observe any permeation events. Since the experimental time scale of SKF release from azosomes is roughly 100 s [13], the simulated and experimental time scales are different by 2×10^8 which might explain why we are unable to observe any permeation events for this larger molecule.
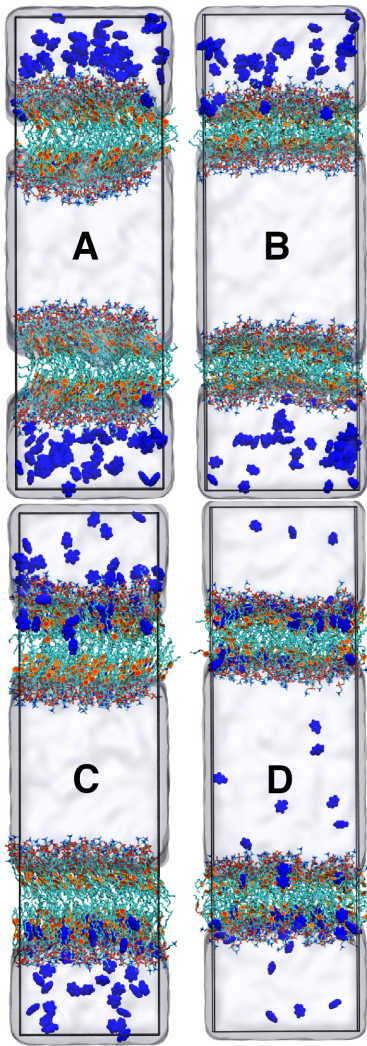
Fig. 12 Snapshots of the azo-PC double bilayer simulations to assess phenol permeation after 1 ns in the *trans* and *cis* isomers (A and B, respectively) and and after 100 ns in the *trans* and *cis* isomers (C and D, respectively). The blue spherical molecules represent the phenol molecules, the cyan atoms are the alkane carbons, the azobenzene moieties are in orange with ring planes filled in, and the clear regions represent water. The hydrogen atoms have been hidden for visual clarity. The periodic cell is drawn in black lines.
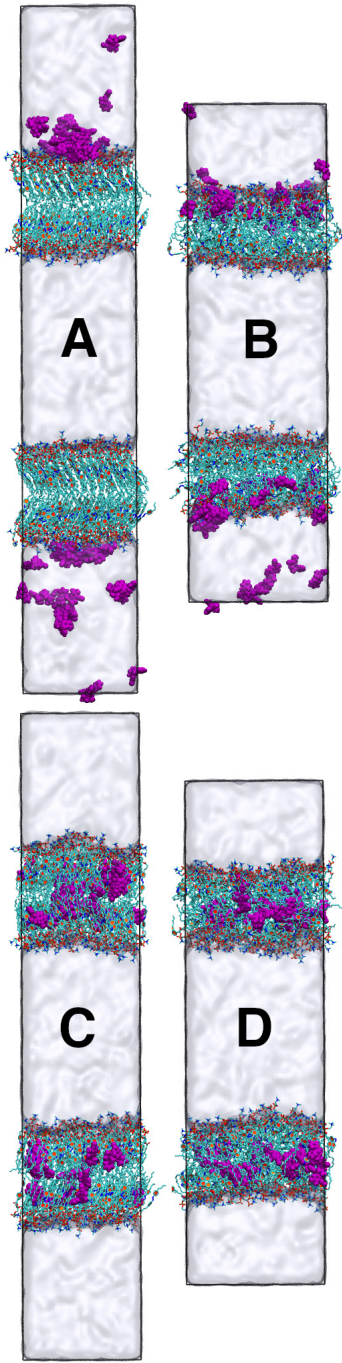

Fig. 13 Snapshots of the azo-PC double bilayer simulations with SKF-81297 after 10 ns in the *trans* and *cis* isomers (A and B, respectively) and and after 500 ns in the *trans* and *cis* isomers (C and D, respectively). The azo-PC lipid carbon, nitrogen, oxygen, and phosphorous atoms are in cyan, blue, red, and gold, respectively, and the hydrogen atoms are hidden for clarity. The azobenzene groups have had their ring planes filled in. The SKF-81297 molecules are drawn in purple spheres. The water regions are rendered colorless, and the periodic cell boundaries are drawn in black.

3.4 Limitations

We based our model on the CHARMM force field which is well-established for phospholipids, and used the azobenzene parameters from the careful study of Böckmann et al. [18] with a modification to specifically select the *cis* or *trans* isomer. Certainly there are other choices for the force field. For example Aleksanyan et al. [39] used the AMBER force field and Maiti et al. [44] used the CHARMM force field with the CGenFF auto-generated parameters for azobenzene. Lyubartsev et al. [45] review the differences between different lipid force fields which show some variation in properties. Due to the small size of the simulation systems (on the order of tens of nanometers in each direction) and the use of periodic boundary conditions, we are forced to simulate a patch of an infinitely extended planar membrane, whereas the experimental systems normally consist of curved (spherical) membranes of diameters on the order of hundreds of nanometers or larger. The lack of curvature in the simulated systems could impose a limitation on what phenomena are observed. Also, the periodic boundary conditions artificially stabilize the membrane against pore formation and rupture, and also suppress long wavelength undulations, which could alter the drug release pathways. Moreover, since we are using fully atomistic molecular dynamics simulations with explicit solvent, the timescale is severely limited. For example, the 500 ns double bilayer simulations with SKF drug molecules are different by 2×10^8 from the experimental timescale of SKF release from azosomes about 100 s as reported by Xiong et al. [13]; this limits our ability to observe permeation events for this larger molecule.

4 Proposed Permeation Mechanism

Our results suggest that *trans*-azo-PC is in a gel-like phase, while *cis*-azo-PC is in a liquid-disordered phase. Thus, we propose that when an azosome undergoes *trans*-to-*cis* isomerization, there is an accompanying gel-to-liquid phase transition that increases the azosome's permeability without the application of heat.

For phenol, the *trans* membrane has a shallow free energy well at the membrane surface so that phenol molecules are attracted there. Then, transition to the *cis* conformer changes the free energy profile, which drives phenol deeper into the membrane. This results in a propensity for phenol to permeate through the membrane under the influence of a chemical potential gradient, even though there is a free energy barrier at the membrane midplane. The two additional local minima present in the phenol *trans* bilayer free energy profile, the higher barrier to cross the membrane midplane, and the intrinsically slower dynamics of the *trans* bilayer lipids all contribute to suppress phenol translocation events. Thus we observe that the isomerization event can effectively activate permeation without the application of heat. In the case of SKF, we also observe two additional local minima in the *trans* bilayer free energy profile, a slightly higher barrier to cross the membrane midplane, and slower lipid dynamics. However, due to the factors discussed above we did not observe permeation events.

Conclusions

In summary, we performed fully atomistic molecular dynamics simulations to study the structure, energetics, and permeability of lipid bilayers composed entirely of azo-PC, a phosphatidylcholine lipid with azobenzene incorporated into one of the two lipid tails. With azobenzene in the *trans* isomer, we found the azo-PC bilayer to be in a gel-like state. A phase transition to the liquid-disordered state occurs when azobenzene transitions to the *cis* isomer, resulting in a bilayer which is thinner and has a larger area per lipid. Also, the liquid-disordered bilayer has an order of magnitude lower bending rigidity although its stretching modulus is unchanged. Isomerization back to the *trans* isomer reverts the bilayer to its gel-like state with repeated isomerization events being completely reversible. The free energy profiles of a model drug, phenol, and a real drug, SKF-81297, crossing the azo-PC bilayer show fewer and lower barriers for the *cis* membrane. By using a double bilayer unit cell to induce a chemical potential gradient across the membrane, we could directly observe phenol permeation through the *cis* bilayer whereas the *trans* bilayer is rather impermeable to phenol. We did not obseve permeation events for SKF-81297 due to the limited timescale of the simulations. These observations would seem to explain, and give mechanistic insight into, the experimental calcein dye release data [13]. In the future, we plan to model multicomponent membranes, as well as mixtures of *trans*-azo-PC and *cis*-azo-PC, to learn more about drug release mechanisms with azosomes.

Author contributions

K.A.A. carried out the molecular dynamics simulations, most of the data analysis, and wrote the original manuscript draft. M.N.H.B. analyzed the bending rigidity and reviewed and edited the entire manuscript. H.X. helped conceptualize the project and reviewed and edited the manuscript. W.S. helped conceptualize the project and reviewed and edited the manuscript. P.A.S. and Z.Q. were responsible for funding acquisition, project administration, resources, and also reviewed and edited the manuscript. S.O.N. supervised the project, helped conceptualize the project, and also reviewed and edited the manuscript.

Conflicts of interest

There are no conflicts to declare.

Data availability

The data supporting this article have been included as part of the Supplementary Information.

Notes and references

1 P. Liu, G. Chen and J. Zhang, *Molecules*, 2022, **27**, 1372.

2 U. Bulbake, S. Doppalapudi, N. Kommineni and W. Khan, *Pharmaceutics*, 2017, **9**, 12.

3 M. Yatvin, J. Weinstein, W. Dennis and R. Blumenthal, *Science*, 1978, **202**, 1290–1293.

4 D. Papahadjopoulos, K. Jacobson, S. Nir and T. Isac, *Biochimica et Biophysica Acta*, 1973, **311**, 330–348.

5 D. Needham, J.-Y. Park, A. M. Wright and J. Tong, *Faraday Discussions*, 2013, **161**, 515–534.

6 J. K. Mills and D. Needham, *Biochimica et Biophysica Acta (BBA) - Biomembranes*, 2005, **1716**, 77–96.

7 A. Yavlovich, B. Smith, K. Gupta, R. Blumenthal and A. Puri, *Molecular Membrane Biology*, 2010, **27**, 364–381.

8 F. Mazur, M. Bally, B. Stadler and R. Chandrawati, *Advances in Colloid and Interface Science*, 2017, **249**, 88–99.

9 D. J. A. Crommelin, P. van Hoogevest and G. Storm, *Journal of Controlled Release*, 2020, **318**, 256–263.

10 Y. Zhao, Z. Ye, D. Song, D. Wich, S. Gao, J. Khirallah and Q. Xu, *Nature Communications*, 2023, **14**, 6645.

11 C. Morgan, E. Thomas, Y. Yianni and S. Sandhu, *Biochimica et Biophysica Acta*, 1985, **820**, 107–114.

12 N. Chander, J. Morstein, J. S. Bolten, A. Shemet, P. R. Cullis, D. Trauner and D. Witzigmann, *Small*, 2021, **17**, 2008198.

13 H. Xiong, K. A. Alberto, J. Youn, J. Taura, J. Morstein, X. Li, Y. Wang, D. Trauner, P. A. Slesinger, S. O. Nielsen and Z. Qin, *Nano Research*, 2023, **16**, 1033–1041.

14 S. D. Pritzl, P. Urban, A. Prasselsperger, D. B. Konrad, J. A. Frank, D. Trauner and T. Lohmüller, *Langmuir*, 2020, **36**, 13509–13515.

15 P. Urban, S. D. Pritzl, D. B. Konrad, J. A. Frank, C. Pernpeintner, C. R. Roeske, D. Trauner and T. Lohmüller, *Langmuir*, 2018, **34**, 13368–13374.

16 J. C. Mathai, S. Tristram-Nagle, J. F. Nagle and M. L. Zeidel, *The Journal of General Physiology*, 2008, **131**, 69–76.

17 L. Martínez, R. Andrade, E. G. Birgin and J. M. Martínez, *Journal of Computational Chemistry*, 2009, **30**, 2157–2164.

18 M. Böckmann, C. Peter, L. D. Site, N. L. Doltsinis, K. Kremer and D. Marx, *Journal of Chemical Theory and Computation*, 2007, **3**, 1789–1802.

19 D. A. Siriwardane, O. Kulikov, B. L. Batchelor, Z. Liu, J. M. Cue, S. O. Nielsen and B. M. Novak, *Macromolecules*, 2018, **51**, 3722–3730.

20 J. B. Klauda, R. M. Venable, J. A. Freites, J. W. O'Connor, D. J. Tobias, C. Mondragon-Ramirez, I. Vorobyov, A. D. MacKerell and R. W. Pastor, *The Journal of Physical Chemistry B*, 2010, **114**, 7830–7843.

21 K. Vanommeslaeghe, E. Hatcher, C. Acharya, S. Kundu, S. Zhong, J. Shim, E. Darian, O. Guvench, P. Lopes, I. Vorobyov and A. D. Mackerell, *Journal of Computational Chemistry*, 2010, **31**, 671–690.

22 W. Yu, X. He, K. Vanommeslaeghe and A. D. MacKerell, *Journal of Computational Chemistry*, 2012, **33**, 2451–2468.

23 K. Vanommeslaeghe and A. D. MacKerell, *Journal of Chemical Information and Modeling*, 2012, **52**, 3144–3154.

24 K. Vanommeslaeghe, E. P. Raman and A. D. MacKerell, *Journal of Chemical Information and Modeling*, 2012, **52**, 3155–3168.

25 J. C. Phillips, D. J. Hardy, J. D. C. Maia, J. E. Stone, J. V. Ribeiro, R. C. Bernardi, R. Buch, G. Fiorin, J. Hénin, W. Jiang, R. McGreevy, M. C. R. Melo, B. K. Radak, R. D. Skeel, A. Singharoy, Y. Wang, B. Roux, A. Aksimentiev, Z. Luthey-Schulten, L. V. Kalé, K. Schulten, C. Chipot and E. Tajkhorshid, *The Journal of Chemical Physics*, 2020, **153**, 044130.

26 W. L. Jorgensen, J. Chandrasekhar, J. D. Madura, R. W. Impey and M. L. Klein, *The Journal of Chemical Physics*, 1983, **79**, 926–935.

27 I. Soteras Gutiérrez, F.-Y. Lin, K. Vanommeslaeghe, J. A. Lemkul, K. A. Armacost, C. L. Brooks and A. D. MacKerell, *Bioorganic & Medicinal Chemistry*, 2016, **24**, 4812–4825.

28 R. Gowers, M. Linke, J. Barnoud, T. Reddy, M. Melo, S. Seyler, J. Domański, D. Dotson, S. Buchoux, I. Kenney and O. Beckstein, *Proceedings of the 15th Python in Science Conference*, 2016, 98–105.

29 N. Michaud-Agrawal, E. J. Denning, T. B. Woolf and O. Beckstein, *Journal of Computational Chemistry*, 2011, **32**, 2319–2327.

30 W. Humphrey, A. Dalke and K. Schulten, *Journal of Molecular Graphics*, 1996, **14**, 33–38.

31 G. Fiorin, M. L. Klein and J. Hénin, *Molecular Physics*, 2013, **111**, 3345–3362.

32 A. Kohlmeyer and J. Vermaas, *TopoTools: Release 1.9*, 2022.

33 W. Rawicz, K. Olbrich, T. McIntosh, D. Needham and E. Evans, *Biophysical Journal*, 2000, **79**, 328–339.

34 T. Giorgino, *Computer Physics Communications*, 2014, **185**, 317–322.

35 G. Khelashvili and D. Harries, *The Journal of Physical Chemistry B*, 2013, **117**, 2411–2421.

36 C. Pernpeintner, J. A. Frank, P. Urban, C. R. Roeske, S. D. Pritzl, D. Trauner and T. Lohmüller, *Langmuir*, 2017, **33**, 4083–4089.

37 A. Manafirad, C. A. Menendez, G. R. Perez-Lemus, S. Thayumanavan, J. J. de Pablo and A. D. Dinsmore, *Langmuir*, 2023, **39**, 15932–15941.

38 M. F. Ober, A. Müller-Deku, A. Baptist, B. Ajanović, H. Amenitsch, O. Thorn-Seshold and B. Nickel, *Nanophotonics*, 2022, **11**, 2361–2368.

39 M. Aleksanyan, A. Grafmueller, F. Crea, V. N. Georgiev, N. Yandrapalli, S. Block, J. Heberle and R. Dimova, *Advanced Science*, 2023, **10**, 2304336.

40 R. M. Venable, F. L. Brown and R. W. Pastor, *Chemistry and Physics of Lipids*, 2015, **192**, 60–74.

41 J. F. Nagle and S. Tristram-Nagle, *Biochimica et Biophysica Acta (BBA) - Reviews on Biomembranes*, 2000, **1469**, 159–195.

42 D. Drabik, G. Chodaczek, S. Kraszewski and M. Langner, *Langmuir*, 2020, **36**, 3826–3835.

43 M. Goral, D. G. Shaw, A. Maczynski and B. Wisniewska-Goclowska, *Journal of Physical and Chemical Reference Data*, 2011, **40**, 033102.

44 A. Maiti and S. Daschakraborty, *Journal of Physical Chemistry B*, 2024, **128**, 7586–7595.

45 A. P. Lyubartsev and A. L. Rabinovich, *Biochimica et Biophysica Acta-Biomembranes*, 2016, **1858**, 2483–2497.

The data supporting this article have been included as part of the Supplementary Information.